could be useful in preventing such losses.

The radionuclide ^{222}Rn, the daughter of ^{226}Ra by alpha emission, should also be subject to release by the exposure of minerals to water. Thus injection of water into formerly dry rock or soil could release a pulse of stored radon. Earth strains prior to earthquakes together with water redistribution which such strains may produce could therefore be responsible for altered radon concentrations associated with earthquakes (*13*). Similarly, the recognition of mechanisms for radon release has implications with respect to the management of uranium tailings.

ROBERT L. FLEISCHER
General Electric Research and Development Center, Schenectady, New York 12301

References and Notes

1. R. L. Fleischer and O. G. Raabe, *Geochim. Cosmochim. Acta* **42**, 973 (1978).
2. K. Kigoshi, *Science* **173**, 47 (1971).
3. A brief summary is given by B. J. Szabo, in *VIII INQUA Conference* (International Union for Quaternary Research, Brussels, 1969), p. 941.
4. R. L. Fleischer, H. W. Alter, S. C. Furman, P. B. Price, R. M. Walker, *Science* **178**, 255 (1972); J. E. Gingrich and J. C. Fisher, in *International Symposium on the Exploration of Uranium Ore Deposits* (International Atomic Energy Agency, Vienna, 1976), pp. 213–224.
5. A. B. Tanner, in *The Natural Radiation Environment*, J. A. S. Adams and W. M. Lowder, Eds. (Univ. of Chicago Press, Chicago, 1964), p. 161.
6. A. A. Levinson and G. L. Coetzee, *Miner. Sci. Eng.* **10**, 19 (1978).
7. W. H. Huang and R. M. Walker, *Science* **155**, 1103 (1967).
8. R. L. Fleischer, P. B. Price, R. M. Walker, *Nuclear Tracks in Solids* (Univ. of California Press, Berkeley, 1975).
9. Implantation is done at a pressure of 5×10^{-3} atm with a source-to-sample separation of 500 μm. The intervening air allows the recoils to pass freely but stops the low-energy sputtered atoms that are expected [P. Sigmund, *Phys. Rev.* **184**, 383 (1969)] from the source.
10. R. L. Fleischer and O. G. Raabe, *Health Phys.* **35**, 545 (1978).
11. R. L. Fleischer, in preparation.
12. J. N. Rosholt and M. Tatsumoto, *Geochim. Cosmochim. Acta* **2** (Suppl. 1), 1499 (1970); *ibid.* **2**, (Suppl. 2), 1577 (1971).
13. M. A. Sadovsky, I. L. Nersesov, S. K. Nigmatullaev, L. A. Latynina, A. A. Lukk, A. N. Semenov, I. G. Simbireva, V. I. Ulomov, *Tectonophysics* **14**, 295 (1972); P. L. Liu, D. K. Wan, T. M. Wan, *Acta Geophys. Sin.* **18**, 279 (1975); A. Mogro-Campero and R. L. Fleischer, *Earth Planet. Sci. Lett.* **34**, 321 (1977); C. Y. King, *Nature (London)* **271**, 516 (1978).
14. I thank L. G. Turner for extensive experimental help. This work was supported by the National Science Foundation.

25 October 1979; revised 5 December 1979

Viscous Flow Circulation of the Solar Wind Behind Venus

Abstract. *A latitudinal circulation model of solar wind flow in the near wake of Venus is presented. It is shown that solar wind fluxes entering through the polar terminator can be viscously forced to lower latitudes. The resulting motion produces a downstream elongation of the nightside polar ionosphere out to the downstream extension of the middle- and low-latitude ionopause. The geometry suggested by this flow circulation model provides a simple explanation of the ionospheric bulge inferred from the Pioneer Venus observations.*

The preliminary results of the plasma probe, magnetometer, electron temperature probe, and ion mass spectrometer experiments carried out with the Pioneer Venus orbiter provided further experimental evidence in support of the deflection into the umbra of the shocked solar wind in the vicinity of the planetary terminator (*1*, *2*). The observed orientation of the magnetic field in the near wake is suggestive of converging flows, which may be confined to the outer regions of the umbra, outside a rarefaction wake extending several Venus radii (*3*). The geometry of the nightside ionopause inferred from the results of the mass spectrometer experiment indicates, in addition, the presence at low latitudes of a prominent ionospheric bulge extending up to ~ 3000 km above the surface. Since the entry of solar wind fluxes into the umbra is a dynamic condition that can be described in terms of a viscous interaction between the shocked solar wind and the ionospheric material (*4*), the question arises whether the presence of such a bulge is compatible with this interpretation. In this report it is shown that this feature can be explained as a result of differences in efficiency of the viscous interaction process, which may be severely diminished at middle and low latitudes by the accumulation of interplanetary magnetic fluxes.

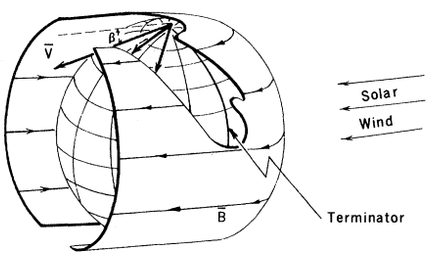

Fig. 1. Schematic diagram of the flow pattern behind Venus. Arrows indicate the motion of ionosheath fluxes entering through the polar regions and subsequently acting against the downstream extension of the middle- and low-latitude ionopause (which is represented by a cylindrical shape). The interplanetary magnetic field lines are shown draped around the dayside ionopause.

Viscous processes are believed to result from a strong dynamic interaction between the shocked solar wind and the ionospheric material. Pseudocollisions resulting from efficient wave-particle interactions should ultimately be responsible for the collective behavior of the plasma and the effective transfer of momentum across the ionopause. An important consequence of this process is a necessary influx of ionosheath particles into the umbra to satisfy conservation of mass flux. This should occur when the kinetic energy density of the local plasma is larger than the energy density of any magnetic field that may permeate the region (*5*). When this condition is not met, the motion of the plasma is controlled by the local magnetic geometry, and thus the plasma is inhibited from interacting dynamically with the stationary ionospheric material. Accumulation of magnetic fluxes of the ionosheath flow around the low- and middle-latitude regions of the planetary ionosphere should impose locally a flow configuration characterized by the latter condition, so that a stable and undeflected inner boundary of the ionosheath flow should exist immediately behind a large section of the terminator (magnetopause-like boundary). At polar latitudes, on the other hand, local enhancement of magnetic fluxes is expected to be significantly smaller, and there should be more efficient dynamic contact between the ionosheath flow and the ionospheric material. These general considerations indicate that the accumulation of interplanetary magnetic field lines around the ionospheric obstacle should result in a more efficient and better developed viscous boundary layer at polar latitudes than at equatorial latitudes.

The preferred access of the ionosheath flow to the umbra through the high-latitude regions of the ionopause should result in the generation of a characteristic circulation flow pattern above the nightside hemisphere. To visualize this, it must be recognized that the region of reduced plasma pressure downstream from the polar terminator is not the only space available for the viscously deviated plasma. The kinetically induced expansion should also proceed laterally into the adjacent regions located underneath the downstream extension of the undeviated ionosheath at middle and low latitudes. This effect is schematically illustrated in Fig. 1, which shows the initial stages of flow penetration from an assumed source in the polar regions. As

0036-8075/80/0229-0981$00.50/0

the (rarefied) fluxes of deviated solar wind particles spill to lower latitudes, they are gradually directed to act, from below, against the undeviated middle- and low-latitude ionosheath fluxes.

The implications of this latitudinal displacement of the solar wind plasma within the umbra should be evident in the resulting distribution of ionospheric material dragged along through viscous action. First, the transfer of momentum to the nightside ionospheric plasma should increase with downstream distance from the polar terminator. As the upper ionosphere is gradually set into motion, it tends to follow (at lower heights) the flow pattern of the solar wind fluxes in the umbra. This concept leads in turn to the suggestion that as such solar wind fluxes are directed against the undeviated ionosheath flow at middle and low latitudes, the accompanying ionospheric material should produce a distinct outward distortion of the geometry of the nightside ionopause. In fact, the kinetic energy acquired by the upper ionospheric plasma may even be sufficient to enable it to protrude into the oncoming middle- and low-latitude ionosheath flow.

An approximate mathematical representation of the position of the ionospheric distortion can be given by determining the intersection of the various vectors drawn from the pole (as shown in Fig. 1) with the downstream extension of the middle- and low-latitude ionopause. The height H above the planet and the latitude λ of the intersection point can be shown to be related to the angle θ away from the terminator plane by

$$\tan\lambda = \frac{\cos^2\theta - \tan^2\beta}{2\tan\beta} \quad (1)$$

$$\frac{R + H}{R + h} = \frac{2\tan\beta \sec\lambda}{\cos^2\theta + \tan^2\beta} \quad (2)$$

where R and h are, respectively, the planetary radius and the ionopause height at the polar terminator and β is the effective deflection angle of the velocity vector into the umbra at the polar terminator. The latitude inferred from Eq. 1 is shown in Fig. 2 for different values of β. The value

$$\beta_{max} = \cos^{-1}[(R + \delta)/(R + h)] = 31°$$

represents the maximum possible effective deflection attained when the velocity vector becomes tangent to the lower ionosphere behind the planetary terminator (it has been assumed that $h \approx 1250$ km and the minimum height reached within the umbra $\delta \approx 200$ km, as suggested by the Pioneer Venus mass spectrometer measurements). The open circles in Fig. 2 show the approximate position of the ionospheric bulge detected in the inbound and outbound ionopause crossings. The latitudes used here ($\lambda \approx 65°$ and 42°) differ from those reported in (*2*) as they refer specifically to the crossings where the bulge is observed rather than to the average latitudes ($\lambda = 50°$ and 20°) of the low-height ionopause intersections (*6*). The θ values are obtained from the reported solar zenith angle values for both crossings.

Aside from the fact that the relative positions of the crossings agree with the predicted dependence of λ on θ, it is notable that the β value required for the high-latitude data is smaller than that suitable for the low-latitude data ($\beta \approx 10°$ and 15°, respectively). This is a consequence of the variation in efficiency of the deflection process with θ. In fact, ionosheath fluxes moving at small angles away from the terminator plane (lateral vectors in Fig. 1) have a smaller kinetic energy density than those oriented at large angles (near the midnight plane) and thus result in a smaller effective deflection into the umbra. The different deflection angle β is also essential for understanding the bulge appearance of the ionospheric distortion when examined along curves of constant latitude [as in figure 2 of (*2*)]. Along one such curve the ionopause height should first increase as weak ionosheath fluxes reach that latitude at an altitude higher than the ionopause height at the terminator. At larger θ values the ionopause height decreases again because of the larger deflection angles β of the more populated and energetic particle fluxes streaming there.

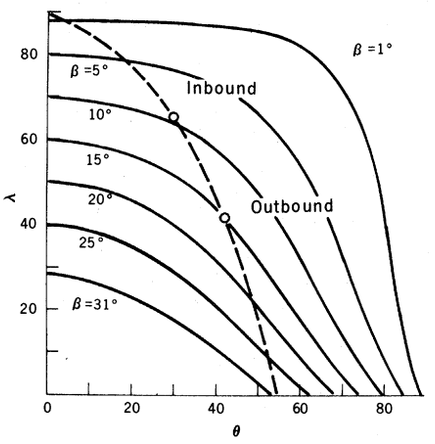

Fig. 2. Calculated values of the latitude λ of the intersection point at the boundary of the cavity as a function of the angle θ away from the terminator plane for selected deflection angles β.

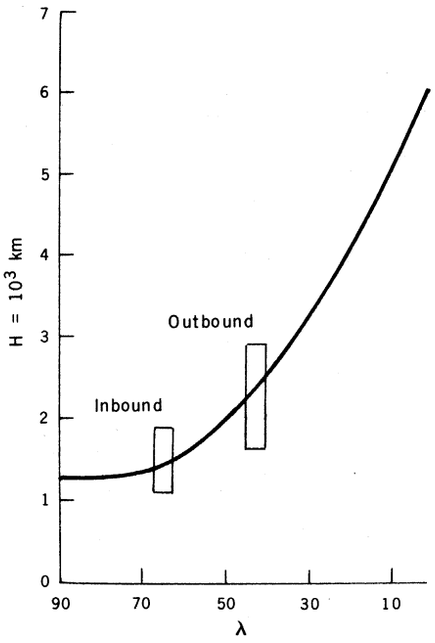

Fig. 3. Predicted height profile of the ionospheric bulge as a function of latitude. The observed height ranges of both ionopause crossings (above the dayside values) are shown for comparison.

The relative positions of the ionospheric crossings in the (λ-θ) plane are particularly significant as they reveal a specific dependence of β on θ, indicated by the dashed curve of Fig. 2. Such a curve must extend from the position $\lambda = 90°$, $\theta = 0°$ [which refers to undeflected ($\beta = 0$) fluxes directed along the terminator plane but restricted to the polar regions] to the position of the bulge in the equatorial plane where β must approach a value slightly smaller than β_{max}. The fact that both crossings of the Pioneer Venus become aligned with respect to these two extreme cases gives the strongest support for the suggested polar entry of ionosheath fluxes into the umbra.

An additional test of the model can be performed by calculating the height of the bulge along this particular curve. The corresponding height profile obtained from Eq. 2 is shown in Fig. 3 together with the approximate height range of both Pioneer Venus crossings. The theoretical values corresponding to the latitudes of the inbound and outbound measurements are $H = 1420$ and 2365 km, respectively. These numbers are in excellent agreement with the experimental observations and further support the validity of the proposed geometry. The same arguments can, in fact, be used to predict that the height and angle θ of the ionospheric bulge in the equatorial plane should reach ~ 6000 km and $\approx 53°$, respectively.

Investigations of the magnetic field orientation (*1*) and plasma flow direction (*3*) in the near wake should provide additional experimental information with which to test these contentions and examine in detail the latitudinal dependence of the nightside ionopause on the direction of the solar wind flow and the interplanetary magnetic field.

H. PÉREZ-DE-TEJADA
Instituto de Geofísica, Universidad Nacional Autónoma de México, México 20, D.F.

References and Notes

1. C. T. Russell, R. C. Elphic, J. A. Slavin, *Science* **205**, 114 (1979).
2. L. H. Brace, H. A. Taylor, Jr., P. A. Cloutier, R. E. Daniell, A. F. Nagy, *Geophys. Res. Lett.* **6**, 345 (1979).
3. D. S. Intriligator, H. R. Collard, J. D. Mihalov, R. C. Whitten, J. H. Wolfe, *Science* **205**, 116 (1979).
4. H. Pérez-de-Tejada and M. Dryer, *J. Geophys. Res.* **82**, 2837 (1976).
5. H. Pérez-de-Tejada, *ibid.* **84**, 1555 (1979).
6. L. Brace, personal communication.
7. On leave at the Instituto de Astronomía, Universidad Nacional Autónoma de Mexico, Ensenada, Baja California. Services and computational facilities provided by the Centro de Investigación Científica y Educación Superior de Ensenada are gratefully acknowledged.

22 July 1979; revised 20 December 1979

Nutrient and Oxygen Redistribution During a Spring Neap Tidal Cycle in a Temperature Estuary

Abstract. *Spring tidal currents produce homogeneous water columns in a number of estuaries that are moderately stratified during neap tides. In the York River estuary, this destratification redistributes ammonium and phosphate regenerated by the benthos as well as oxygen from the surface. This redistribution has significant implications for nutrient cycles, organism distributions, and the management of estuaries.*

Estuaries are characterized on the basis of their morphometry and salinity structure (*1*). For example, Pritchard (*2*) has conceptually modeled estuarine types according to three different density-stratification and circulation patterns: highly stratified (type A), moderately stratified (type B), and vertically homogeneous (type C). In contrast to highly stratified estuaries, vertically homogeneous ones are expected to be shallow, wide, and dominated by tidal currents rather than freshwater input (*3*). The Chesapeake Bay and its tributaries have been considered classical examples of moderately stratified estuaries. Indeed, when this system is viewed in the long-term average sense (that is, month to month), its salt distribution is well explained by such a model.

Recently, Haas (*4*) discovered that at least portions of the Chesapeake estuarine system alternate between vertical homogeneity and stratification within a time scale of days. Such a short time scale is an appropriate one for those seeking a relationship between biological or chemical processes and estuarine hydrography. Haas's analysis of the observed oscillation cycle of the York, James, and Rappahannock rivers revealed a strong positive correlation between destratification events and spring tidal height; thus these destratification events are predictable. Destratification at the mouth of the York River was most intense about 4 days after maximum spring high tides, and stratification was most evident during neap tidal periods. Surprisingly, neither short-term variation in freshwater flow nor meteorological events had much bearing on the occurrence of vertical mixing.

This report concerns the effects and implications of spring tidal destratification phenomenon on nutrient and O distributions in the York River during August 1978 (*5*).

We conducted intensive sampling of the water column during periods of neap tidal stratification (7 to 17 August), spring tidal destratification (21 to 24 August), and subsequent neap tidal restratification (24 to 31 August). Vertical profiles for NO_2^-, NH_4^+, PO_4^{3-}, and O strongly reflected the stratification state of the estuary (Fig. 1), which was primarily due to the salinity and not the temperature component of density (sigma t). During the first stratification period, O and NO_2^- concentrations were high above the halocline and low below it (Fig. 1, B and D) whereas the reverse was true for NH_4^+ (Fig. 1E) and PO_4^{3-} (Fig. 1C) (*6*). The destratification event, characterized by a virtually uniform distribution with depth of all constituents

Table 1. Mean water column concentrations (± standard deviation) for hydrocasts at the mouth of the York River for the range of days in August 1978; $\Delta\overline{X}$ is the salinity difference between top and bottom; ΣN is the sum of NO_2^-, NO_3^-, and NH_4^+. The N and P concentrations are in microgram atoms per liter. The numbers in parentheses indicate the number of hydrocasts averaged.

Date	$\Delta\overline{X}$ (per mil)	$\overline{X}$ (per mil)	$\overline{X}\,\Sigma N$	$\overline{X}\,PO_4^{3-}$	$\overline{X}\,NO_2^- + NO_3^-$	$\overline{X}\,NH_4^+$
7 to 17	3.94 ± 1.10 (13)	21.3 ± 0.33 (13)	9.85 ± 2.50 (11)	0.39 ± 0.11(10)	3.17 ± 1.27 (11)	6.68 ± 1.36 (11)
21 to 24	0.15 ± 0.39 (10)	20.4 ± 0.24 (10)	3.00 ± 0.81 (10)	0.27 ± 0.08(9)	1.40 ± 0.61 (10)	1.50 ± 0.51 (10)
24 to 31	5.43 ± 1.51 (9)	22.9 ± 1.88 (9)	8.30 ± 2.14 (9)	0.80 ± 0.46(8)	1.12 ± 0.77 (9)	7.18 ± 2.54 (9)

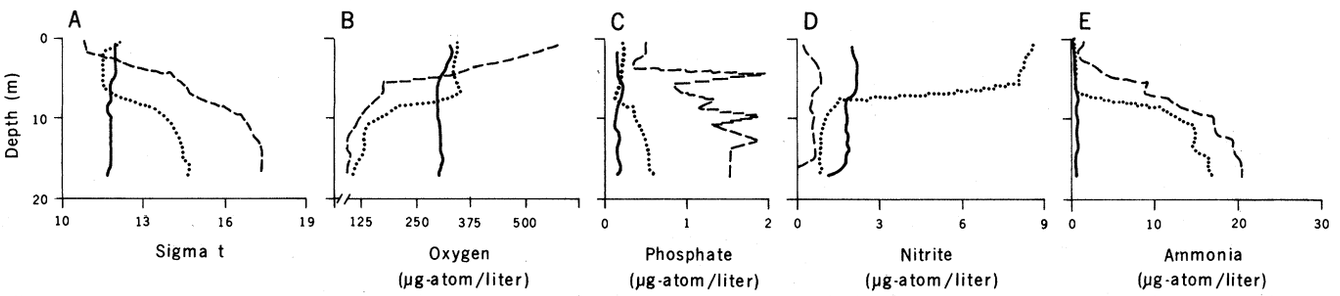

Fig. 1. Profiles of (A) sigma t, (B) oxygen, (C) phosphate, (D) nitrite, and (E) ammonia for 10 August (.....), 23 August (_____), and 29 August (------). Profile depths vary slightly because of tidal fluctuation and slight positional changes of the vessel.

0036-8075/80/0229-0983$00.50/0